Total X-ray Scattering

Masatsugu Yoshimoto*

Abstract
Total scattering measurement is widely used to evaluate the local structure of the cathode and the solid electrolyte for Li-ion batteries. The observed pair distribution function $G_{obs}(r)$ obtained from the Fourier transform of the structure factor $S(Q)$ has information not only about neighboring distances but also about the coordination numbers and the number density of sample. Herein, we discuss deviations in $G_{obs}(r)$ arising from the standard deviation of $S(Q)$ and the termination error of the measurable maximum and minimum scattering vector in $G_{obs}(r)$ using the basic theory of total scattering analysis.

Keywords: total X-ray scattering, PDF analysis, Error propagation, Density estimation.

Introduction

Locally disordered crystalline materials have been used recently as key components of secondary batteries and electronic materials. In a crystalline material, powder X-ray diffraction analysis, which includes Rietveld analysis, the DD method and the FP method, is powerful method for the quantitative analysis of crystalline phase and crystallite size. In contrast, the local structure of amorphous materials, which is difficult to analyze by powder X-ray diffraction analysis, can be evaluated by total X-ray scattering and pair distribution function PDF analysis.

The pair distribution function $G_{obs}(r)$ is obtained from the Fourier transform of the observed structure factor $S(Q)$[1]. The peak positions in $G_{obs}(r)$ indicate the distances between neighboring atoms. Furthermore, a structural model (e.g. crystal structure model, cluster model, molecular model) is required when $G_{obs}(r)$ peaks are discussed in detail using partial correlations. Both high quality $G_{obs}(r)$ and a reasonable structural model are important to evaluate the detailed local structure. We have reported that the total scattering functions ($S(Q)$ and $G_{obs}(r)$) can determine the atomic-scale density and the cluster (polyhedron) shape from oscillations in the high-Q region. Reverse Monte Carlo (RMC) refinement is powerful technique to construct a proper structural model from the experimental data[2],[3]. We have released the Total X-ray Scattering (TXS) plugin[4] as part of SmartLab Studio II as an analysis tool for total scattering profiles, including RMC modeling, accessible to by wide variety of users from beginner to professional.

In this paper, we discuss three topics: 1. the procedure of $S(Q)$ and $G_{obs}(r)$ calculation from the observed total scattering intensity, 2. evaluation of signal to noise in $G_{obs}(r)$ using the uncertainly calculated from $S(Q)$, and 3. evaluation of termination error in $G_{obs}(r)$.

* X-ray Research Laboratory, Rigaku Corporation.

Methods

The basic theory of total scattering measurement

The pair distribution function $G(r)$ is obtained from the Fourier transform of the structure factor $S(Q)$ as follows:

$$G(r) = \frac{2}{\pi}\int_0^\infty Q\left[S(Q)-1\right]\sin Qr\, dQ. \quad (1)$$

where r is inter-atomic distance and Q is the scattering vector defined in Eq. 2.

$$Q = \frac{4\pi\sin\theta}{\lambda}. \quad (2)$$

where θ is half of scattering angle 2θ and λ is the X-ray wavelength. The experimental pair distribution function $G_{obs}(r)$ is obtained from Eq. 3 where $S(Q)$ is measured over a finite range

$$G_{obs}(r) = \frac{2}{\pi}\int_{Q_{min}}^{Q_{max}} Q\left[S(Q)-1\right]\sin Qr\, dQ \quad (3)$$

where Q_{min} and Q_{max} are the scattering vectors corresponding to the minimum and maximum value of the measurement, respectively. According to Eq. 2, the total scattering profile with a wide range of Q can be measured by short-wavelength X-rays. It is widely known that the peak width of $G_{obs}(r)$ becomes sharper with decreasing X-ray wavelength. Furthermore, the peak width of $G_{obs}(r)$ relates to the spatial resolution Δr calculated from Q_{max} as follows:

$$\Delta r = \frac{\pi}{Q_{max}}. \quad (4)$$

$\Delta\rho$ for each specific X-ray wavelength can be easily calculated when $2\theta = 180°$ is used

$$\Delta r \approx \frac{\lambda}{4}. \quad (5)$$

Table 1 lists Δr calculated using Eq. 5 for X-ray

Table 1. The spatial resolution Δr of each specific X-ray calculated by Eq. 3.2.

Specific X-ray	wavelength λ (Å)	The spatial resolution Δr (Å)
Ag Kα	0.5609	0.14
Mo Kα	0.7107	0.18
Cu Kα	1.5418	0.38

wavelengths frequently used with laboratory instruments. From this it can be seen that Ag Kα and Mo Kα radiations are suitable X-ray sources for total scattering measurements using a laboratory instrument.

The observed total scattering intensity is composed of several parts:

$$I_{obs}=I_{coh}+I_{inc}+I_{bg}+I_{XRF} \tag{6}$$

where I_{coh} is the coherent scattering intensity of sample, I_{inc} is the incoherent scattering intensity of sample, I_{bg} is the background intensity from a blank container and air and I_{XRF} is the X-ray fluorescence intensity from sample.

I_{bg} should be lower than the scattering intensity of the sample ($I_{coh}+I_{inc}$). For X-ray total scattering, borosilicate glass capillaries are suitable as a measurement container at room temperature. It is difficult to correct the effect of I_{XRF} on total scattering intensity. Therefore, the incident X-ray energy should be selected so that it does not exceed the absorption edge of each element in the material under investigation or is sufficiently high.

The total scattering intensity of a sample can be derived using I_{obs}, I_{bg}, A_{obs} and A_{bg}:

$$I_{sample}=\frac{1}{P}\left(\frac{I_{obs}}{A_{obs}}-\frac{I_{bg}}{A_{bg}}\right). \tag{7}$$

A is the absorption factor. Typical sample shapes and their absorption factors are summarized below:

Flat plate

a. Absorption factor for Bragg–Brentano geometry (thick sample; $\mu t \gg 1$)

$$A=\frac{1}{2\mu}. \tag{8.1}$$

b. Absorption factor for transmission geometry with $2\theta/\theta$ measurement

$$A=\frac{t}{\cos\theta}\exp\left(-\frac{\mu t}{\cos\theta}\right). \tag{8.2}$$

Cylindrical shape (glass capillary)

The absorption factor uses the absorption coefficients published in *International Tables for X-ray Crystallography Vol. C* [5].

The polarization factor P is defined in Eq. 9

$$P=\frac{\alpha+(1-\alpha)\cos^2 2\theta}{2}. \tag{9}$$

where α is the polarization rate of the incident X-ray in the direction perpendicular to the scattering plane. α is 0.5 when a laboratory instrument is used. The structure factor $S(Q)$ is calculated using I_{sample}, atomic scattering factors and the Compton scattering intensity of the sample

$$S(Q)=\frac{aI_{sample}-(\langle f^2\rangle+I_{inc})+\langle f\rangle^2}{\langle f^2\rangle}, \tag{10}$$

where I_{inc} is the Compton scattering intensity. $\langle f^2\rangle$ and $\langle f\rangle$ are defined in Eq. 11

$$\langle f^2\rangle=\sum_i c_i f_i^2, \langle f\rangle=\sum_i c_i f_i. \tag{11}$$

c_i and f_i is the i-th atomic molar fraction and atomic scattering factor, respectively.

a is a normalizing coefficient to the atomic scattering factor calculated from the formula[6],[7] defined below

$$a=\frac{-2\pi^2\rho_0+\int_{Q_{min}}^{Q_{max}}\frac{Q^2(\langle f^2\rangle+I_{inc})}{\langle f\rangle^2}dQ}{\int_{Q_{min}}^{Q_{max}}\frac{Q^2 I_{sample}}{\langle f\rangle^2}dQ}. \tag{12}$$

Eq. 12 is called Krogh-Moe-Norman method.

Error propagation in $G_{obs}(r)$

Thijsse, Tody and Egami have reported the error propagation from $S(Q)$ to $G_{obs}(r)$ caused by intensity fluctuation in the observed profile[8]–[10]. For detailed derivations, please refer to references (8)–(10). $\delta G^2_{obs}(r)$, which is the standard deviation in $G_{obs}(r)$, is calculated from the eqation below:

$$\delta G^2_{obs}(r)=\frac{4}{\pi^2}\sum_i \delta S^2(Q_i)Q_i^2\sin^2 Q_i r\Delta Q_i^2, \tag{13}$$

where ΔQ_i is the step size between measured point abd $\delta S(Q_i)$ is the standard deviation for $S(Q)$ as defined below

$$\delta S(Q)=ab\frac{\sqrt{I_{obs}(Q)}}{A_{obs}P}. \tag{14}$$

where a is the normalizing coefficient calculated from the Krogh–Moe–Norman method shown in Eq. 12, b is the scaling coefficient used in data processing until the intensity is normalized to the atomic scattering factor. (i.e., the scaling coefficient when the profiles merge), A_{obs} is the absorption factor of the sample, and P is the polarization factor.

The termination error in finite Q range on $G_{obs}(r)$

Since $G_{obs}(r)$ is only part of $G(r)$, Eq. 1 is rewritten using Eq. 3 below:

$$G(r) = \frac{2}{\pi}\int_0^{Q_{\min}} Q\{S(Q)-1\}\sin Qr\, dQ + \frac{2}{\pi}\int_{Q_{\min}}^{Q_{\max}} Q\{S(Q)-1\}\sin Qr\, dQ + \frac{2}{\pi}\int_{Q_{\max}}^{\infty} Q\{S(Q)-1\}\sin Qr\, dQ.$$

$$\therefore G_{\text{obs}}(r) = G(r) - \frac{2}{\pi}\int_0^{Q_{\min}} Q\{S(Q)-1\}\sin Qr\, dQ - \frac{2}{\pi}\int_{Q_{\max}}^{\infty} Q\{S(Q)-1\}\sin Qr\, dQ. \quad (15)$$

In the next section, we introduce the effect of the termination error caused by $Q_{\max}$ and $Q_{\min}$ on $G_{\text{obs}}(r)$.

Termination error due to $Q_{\max}$ within $G_{\text{obs}}(r)$

As described in Eq. 15, $S(Q)$ has a finite Q range ending at $Q_{\max}$. Therefore, a fringe in the form of a sinc function appears around the peaks of $G_{\text{obs}}(r)$ as follows:

$$f(r) = \frac{\sin\left(Q_{\max}(r-r_0)\right)}{(r-r_0)}. \quad (16)$$

where r_0 is the peak position. The fringe caused by $Q_{\max}$ termination error is called a side lobe. To reduce the side lobe effect on $G_{\text{obs}}(r)$, a Lorch-type window function [11] is widely used when $G_{\text{obs}}(r)$ is obtained via Fourier transforms from $S(Q)$. The Lorch-type window function is defined below

$$W(Q) = \frac{\sin\left(\frac{\pi Q}{Q_{\max}}\right)}{\frac{\pi Q}{Q_{\max}}}. \quad (17)$$

Termination error due $Q_{\min}$ within $G_{\text{obs}}(r)$

According to the second term in Eq. 15, the termination error arising from $Q_{\min}$ affects the $G(r)$ profile. This problem can be resolved if the data in $0 \le Q < Q_{\min}$ range is estimated. It is widely known that $S(0)$ relates to isothermal compressibility[12]. The data can be provided by interpolation between $S(0)$ and $S(Q_{\min})$, when the isothermal compressibility of the sample is available. For most samples, it is difficult to obtain the isothermal compressibility value. Therefore, we propose another method to approximate the termination error caused by $Q_{\min}$. Changes in $S(Q)$ between 0 and $Q_{\min}$ can be considered constant (i.e., $S(Q_{\min})$) if the measured $Q_{\min}$ value is sufficiently small. In other words, this assumption is reasonable when the system is considered to be homogeneous over a sufficiently large distance. For example, when the minimum scattering angle is $2\theta = 3°$, the corresponding $Q_{\min}$ value for an X-ray wavelength of $\lambda_{\text{Ag K}\alpha} = 0.5609$ Å and $\lambda_{\text{Mo K}\alpha} = 0.7107$ Å is $Q_{\min,\,\text{Ag K}\alpha} = 0.587\,\text{Å}^{-1}$ and $Q_{\min,\,\text{Mo K}\alpha} = 0.463\,\text{Å}^{-1}$, respectively. These values are considered sufficiently low, so Eq. 15 can be approximated as follows:

$$G(r) \approx \frac{2}{\pi}\{S(Q_{\min})-1\}\int_0^{Q_{\min}} Q\sin Qr\, dQ + \frac{2}{\pi}\int_{Q_{\min}}^{Q_{\max}} Q\{S(Q)-1\}\sin Qr\, dQ = \frac{2}{\pi}\{S(Q_{\min})-1\}\left(\frac{\sin Q_{\min} r}{r^2} - \frac{Q_{\min}\cos Q_{\min} r}{r}\right) + \frac{2}{\pi}\int_{Q_{\min}}^{Q_{\max}} Q\{S(Q)-1\}\sin Qr\, dQ. \quad (18)$$

Finally, we obtain $G_{\text{obs}}(r)$ with minimized termination error by applying Eq. 18 during the Fourier transform of $S(Q)$. Furthermore, the contribution of the termination error in $G_{\text{obs}}(r)$ due to $Q_{\min}$ can be estimated using the following:

$$\gamma(r) = \frac{2}{\pi}\{S(Q_{\min})-1\}\left(\frac{\sin Q_{\min} r}{r^2} - \frac{Q_{\min}\cos Q_{\min} r}{r}\right). \quad (19)$$

Experimental Section

The total scattering measurements were performed using a SmartLab® diffractometer equipped with a HyPix-3000 HE detector. The scattering angle 2θ was scanned from 3.0° to 156°, corresponding to a scattering vector Q range from $0.587\,\text{Å}^{-1}$ to $21.918\,\text{Å}^{-1}$. Ag Kα incident X-rays ($\lambda = 0.5609$ Å, $E_{\text{Ag K}\alpha} = 22.11$ keV) were monochromatized by an elliptic d-space graded multilayer mirror (CBO-E (Ag)) and focused on the detector position. The specimen was a SiO_2 glass rod with a diameter of $\phi = 0.5$ mm, purchased from Nakahara Opto-Electronics Laboratories, Inc. The air scattering profile was used as background. To evaluate the contribution of the standard deviation on $G_{\text{obs}}(r)$, two datasets were prepared with different measurement times: one with a short measurement time of 3 min, and the other with a long measurement time of 8 hours. $S(Q)$ was obtained from the total scattering profiles by applying Eqs. 7 through 12.

Results and Discussion

The evaluation of error propagation from $S(Q)$ to $G_{\text{obs}}(r)$

Figure 1 shows the coherent scattering intensity of SiO_2 glass normalized to the atomic scattering factor, with a measurement time of 8 hours. The observed total scattering profile contains only the SiO_2 glass signal with no other contributions such as air and parasitic scattering. Figure 2 shows the comparison of $S(Q)$ with the different measurement times and the corresponding standard deviation. $S(Q)$ obtained from a 3-minute measurement shows a slight signal from SiO_2 glass, while the standard deviation exceeds the signal of SiO_2 glass meso-scale structure. In contrast, the $S(Q)$ obtained from an 8-hour measurement clearly shows the SiO_2 glass signal with a relatively low standard deviation. Figure 3 shows $G_{\text{obs}}(r)$ with the standard deviation ($\pm 2\sigma$) calculated using Eq. 13, shown as a dashed line.

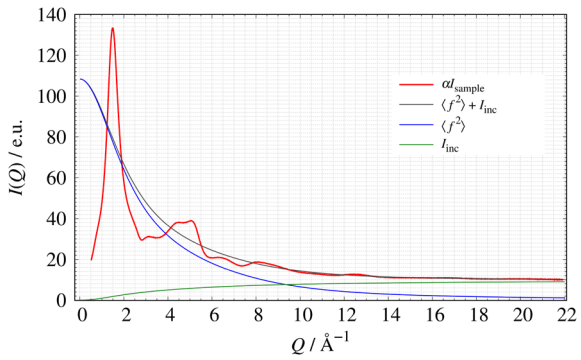

Fig. 1. Comparison of the coherent scattering intensity of SiO_2 glass and the atomic scattering factor of SiO_2. Red: the coherent scattering intensity of SiO_2 glass, blue: the atomic scattering factor of SiO_2 $\langle f^2 \rangle$, green: the Compton intensity $I_{Compton}$, black: the sum of $\langle f^2 \rangle + I_{inc}$.

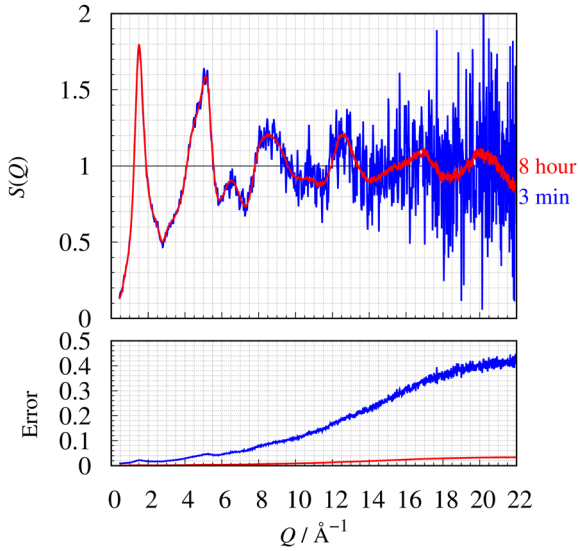

Fig. 2. Comparison of SiO_2 glass $S(Q)$ at different measurement times. Blue: 3 min., red: 8 hours. The bottom graph also shows the standard deviation raised from the intensity fluctuations calculated by Eq. 14.

$S(Q)$ with a low standard deviation provides $G_{obs}(r)$ that exhibits clear peaks up to around $r = 7$ Å.

To compare the contribution of standard deviation to the total scattering profile in the high-Q region, two datasets were collected: One is obtained as a single continuous profile, which is called a "scanning measurement". The other collects the total scattering profile by dividing it into several regions, which is called the "dividing measurement." By using a dividing measurement, the total scattering intensity is almost constant over the entire wide Q range. The measurement conditions of both datasets are listed in Table 2. $S(Q)$ and the corresponding standard deviation for both measurements are shown in Figure 4. The standard deviation of the dividing measurement at $Q \geq 19$ Å^{-1} is lower than that of the scanning measurement. At $Q < 19$ Å^{-1}, the measurement time for the dividing measurement is slightly shorter than for the scanning

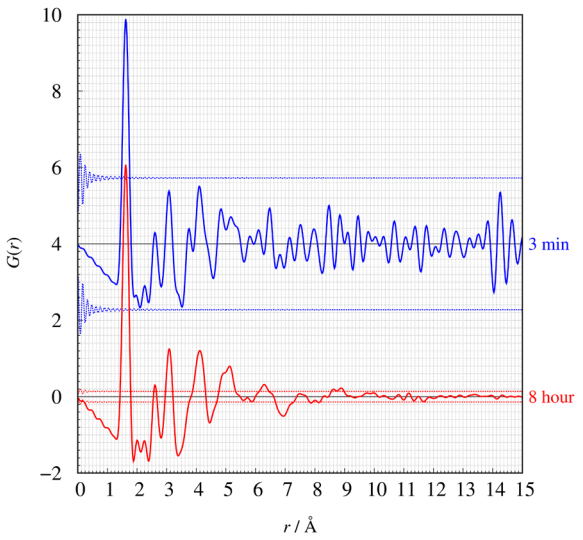

Fig. 3. Comparison of SiO_2 glass $G_{obs}(r)$ at different measurement times. Blue: 3 min., red: 8 hours. The dashed line in the graph indicates the standard deviation ($\pm 2\sigma$) in $G_{obs}(r)$ calculated from Eq. 13.

Table 2. Measurement conditions of scanning measurement and dividing measurement.

Sequence No.	Scanning measurement	Dividing measurement
1	2°–156.6° 1°/min × 3 scan	2°–25° 5°/min × 1 scan
2		20°–75° 2°/min × 3 scan
3		75°–120° 1°/min × 3 scan
4		115°–156.6° 1°/min × 4 scan
Total time (h)	8	7.6

measurement, as shown in Table 2. As a result, the standard deviation of the dividing measurement in this region is higher than the scanning measurement. Figure 5 shows $G_{obs}(r)$ and the corresponding deviation obtained from each $S(Q)$ and $\delta S(Q)$. Both $G_{obs}(r)$ are almost same, and we cannot detect any differences in the effect of the standard deviation in the low-Q region. According to these results, it is suggested that the deviation in $G_{obs}(r)$ is strongly affected by the standard deviation $\delta S(Q)$ in the high-Q region.

To summarize, the deviation calculated from the standard deviation in observed intensities enables a quantitative evaluation about whether $G_{obs}(r)$ indicates a signal or not.

Evaluation of Q_{max} termination error in $G_{obs}(r)$

To compare the contribution of the standard deviation in $G_{obs}(r)$, two $G_{obs}(r)$ profiles—one with and one without applying a Lorch-type window function—are shown in Fig. 6. The window function helps surpress a side lobe raised around peaks in $G_{obs}(r)$. It can be observed that the window function affects $G_{obs}(r)$ by reducing peak heights and creating broader peak widths

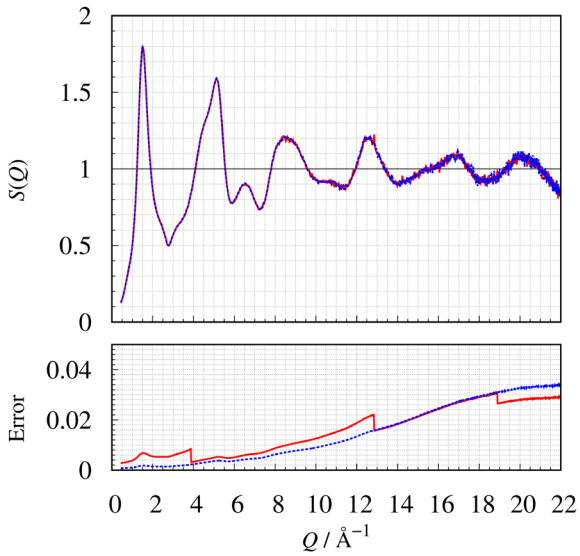

Fig. 4. Comparison of $S(Q)$ of SiO_2 glass using different measurement methods. Red: dividing measurement, blue: scanning measurement.

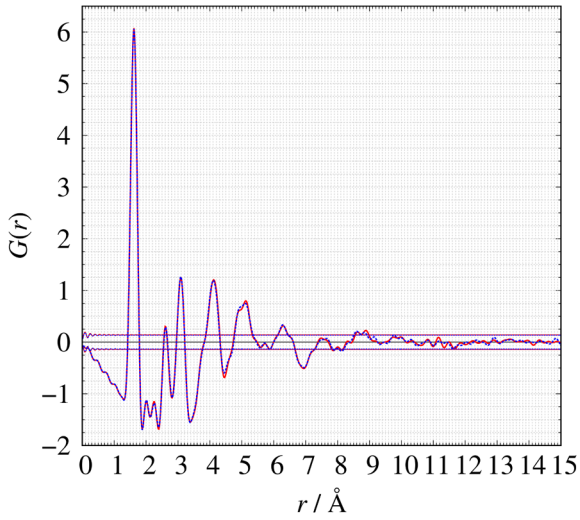

Fig. 5. Comparison of $G_{obs}(r)$ of SiO_2 glass using different measurement methods. Red: dividing measurement, blue: scanning measurement.

than $G_{obs}(r)$ without the window function.

We demonstrate the relationship between peak and side lobe using $G_{obs}(r)$ of SiO_2 glass and the SiO_4 correlation. SiO_4 correlation $G_{SiO_4}(r)$ in SiO_2 glass is calculated by the following equation

$$G_{SiO_4}(r) = \frac{2}{\pi}\int_0^{Q_{max}} \left\{ 4\frac{2c_{Si}f_{Si}f_O}{\langle f\rangle^2}\frac{\sin Qr_{SiO}}{r_{SiO}} + 6\frac{c_O f_O f_O}{\langle f\rangle^2}\frac{\sin Qr_{OO}}{r_{OO}} \right\} dQ, \quad (20)$$

where r_{SiO} and r_{OO} is the distance of Si–O correlation and O–O correlation, respectively. When a SiO_4 cluster is assumed to adopt a tetrahedral form, $r_{OO}=\sqrt{8/3}r_{SiO}$. Therefore, Eq. 20 is modified as follows

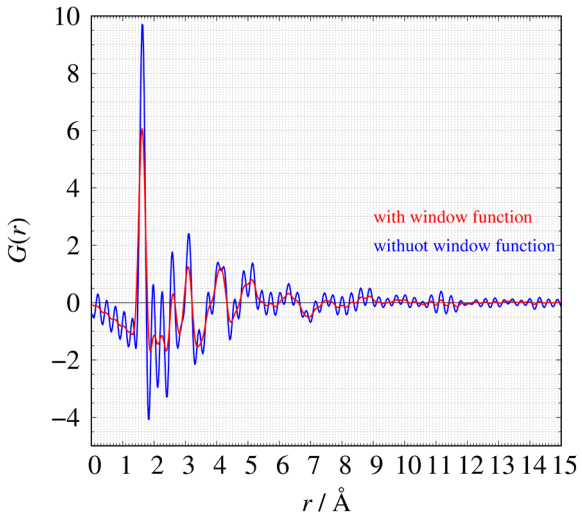

Fig. 6. Comparison of SiO_2 glass $G_{obs}(r)$. Red: with Lorch-type window function, blue: without Lorch type-window function.

$$G_{SiO_4}(r) = \frac{2}{\pi}\int_0^{Q_{max}} \left\{ 4\frac{2c_{Si}f_{Si}f_O}{\langle f\rangle^2}\frac{\sin Qr_{SiO}}{r_{SiO}} + 6\frac{c_O f_O f_O}{\langle f\rangle^2}\frac{\sin Q\sqrt{8/3}r_{SiO}}{\sqrt{8/3}r_{SiO}} \right\} dQ. \quad (21)$$

We calculate $G_{SiO}(r)$と$G_{OO}(r)$と$G_{SiO_4}(r)$ using $r_{SiO}=1.62$ Å calculated from the first peak position on $G_{obs}(r)$.

Figures 7a and 7b show $G_{obs}(r)$ at the maximum measurable Q value of each $Q_{max}=22.0$ Å^{-1}, 17.4 Å^{-1}. The 1st and 2nd peaks of $G_{obs}(r)$ are consistent with the Si–O and O–O correlations calculated from a SiO_4 tetrahedron. The result indicates that SiO_4 tetrahedra remain in the SiO_2 glass structure. In Figs 7a and 7b, $G_{obs}(r)$ shows two and one small peaks, respectively, in the range of 1.9 Å$<r<$2.3 Å . Comparing calculated $G_{SiO}(r)$ and $G_{OO}(r)$ of a SiO_4 cluster, they are side lobes of the termination error caused by Q_{max}. By using a cluster model, the oscillation raised in the small r region can indicate whether it is the signal from the sample or a side lobe due to termination error caused by Q_{max}. However, there are few cases to simply express correlation such as a SiO_4 tetrahedron. Therefore, another method without a cluster model is required to evaluate the relationship between the peak and side lobes from termination error due to Q_{max}. Sinc function $f(r)$ defined in Eq. 16 is equal to $f(r)=Q_{max}$ when $r-r_0=0$. The 1st positive side lobe is observed at $r-r_0=\pm 5\pi/2Q_{max}$. The contributions of the side lobe at the 1st and 2nd peaks can be evaluated by the ratio of the 1st positive side lobe height to the peak height; the ratio is approximately 0.127. The height of a small oscillation around $r=2.0$ Å shown in Figs. 7a and 7b is less than 12.7% of the 1st peak height at r=1.62 Å. Therefore we conlucde that the small oscillation is a side lobe from the termination error caused by Q_{max}. To

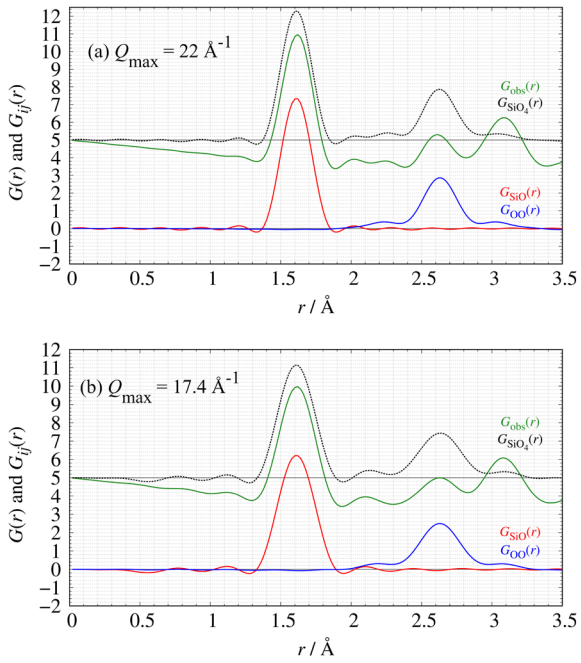

Fig. 7. SiO_2 glass $G_{obs}(r)$ (green solid line), $G_{SiO_4}(r)$ of SiO_4 tetrahedron (black solid line), Si–O partial correlation $G_{SiO}(r)$ (red solid line) and O–O partial correlation $G_{OO}(r)$ (blue solid line). (a): Q_{max}=22.0 Å^{-1}, (b): Q_{max}=17.4 Å^{-1}.

summerize, we carefully evaluated the small oscillations in $G_{obs}(r)$ to determine whether these signal are from the sample or the termination error of Q_{max}.

Evaluation of Q_{min} termination error in $G_{obs}(r)$

Liquid Ar

To validate the contribution of Q_{min} termination error in $G_{obs}(r)$, $S(Q)$ of liquid Ar reported by Yarnell[13] is used as demonstration data. Figure 9 shows the $G_{obs}(r)$ obtained from the Fourier transform of each $S(Q)$ shown in Fig. 8. Small oscillations arise over a wide r-range of $G_{obs}(r)$ calculated from $S(Q)$ in $Q \geq 0.5$ Å^{-1} compared to $G(r)$ from $Q \geq 0$ Å^{-1}. The frequency and amplitude of the oscillation calculated by Eq.19 is consistent with those of the residual curve shown in Fig. 9. In Fig. 11, the blue dashed line shows $G(r)$ calculated by Eq. 18, while the red solid line shows $G(r)$ calculated from $S(Q)$ with $Q \geq 0$ Å^{-1}, which is shown in Fig. 8. The residual curve between $G(r)$ calculated by each method is almost zero. According to the result, the present method applying Eq. 18 provides $G(r)$ corrected for the Q_{min} termination error.

Improved density estimation results by applying the Q_{min} termination error correction

The termination error of Q_{min} shows a large modulation around the 1st peak of $G_{obs}(r)$ as shown in Figs. 9 and 10. We have reported that the number density of a sample can be estimated using $G_{obs}(r)$ less than the 1st peak position when the total scattering profile is obtained correctly[2]. We have assumed that the termination error of Q_{min} was negligible compared to the signal from the sample. Therefore, the number

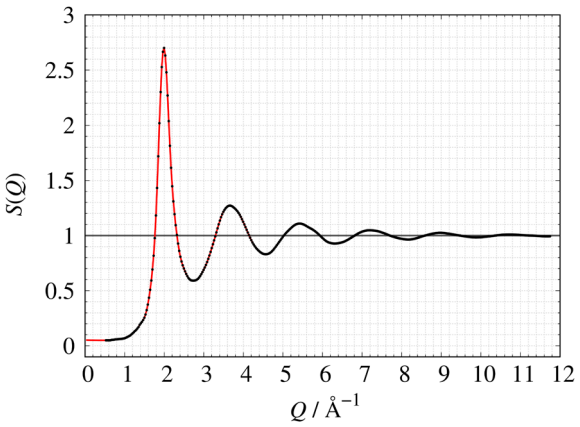

Fig. 8. Comparison of $S(Q)$ of liquid Ar. Red line: $S(Q)$ with 0 Å$^{-1} \leq Q \leq$ 11.75 Å^{-1} and black filled circle: $S(Q)$ with 0.5 Å$^{-1} \leq Q \leq$ 11.75 Å^{-1}.

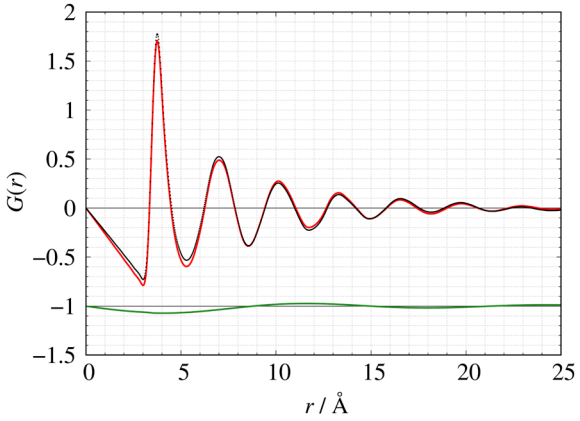

Fig. 9. Comparison of $G(r)$ of liquid Ar. Red solid line: $G(r)$ obtained from $S(Q)$ with 0 Å$^{-1} \leq Q \leq$ 11.75 Å^{-1}, black filled circle: $G_{obs}(r)$ obtained from $S(Q)$ with 0.5 Å$^{-1} \leq Q \leq$ 11.75 Å^{-1} and green solid line: the difference curve between $G_{obs}(r)$ and $G(r)$.

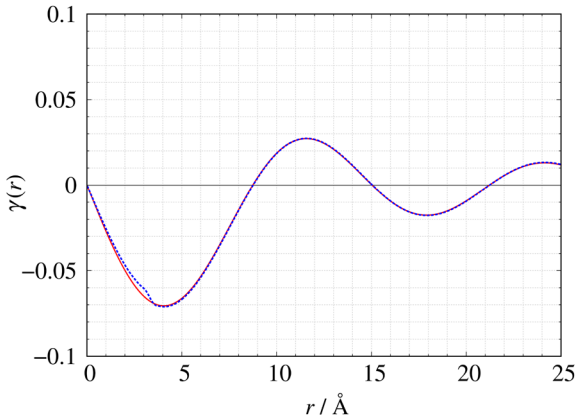

Fig. 10. Comparison of contribution of the termination error of Q_{min} and the difference curve shown in Fig. 9.

density was calculated from $S(Q)$ without the Q_{min} termination error correction. We notice that the density estimation method can provide better accuracy for the reference material by applying the Q_{min} termination error

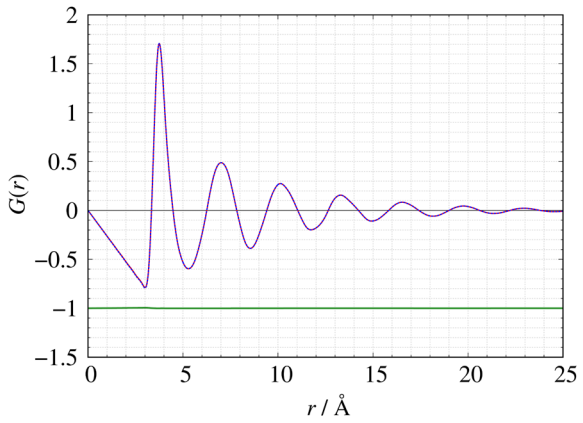

Fig. 11. Comparison of $G(r)$ of liquid Ar after and before correction of Q_{min} termination error. red solid line: $G(r)$ calculated from $S(Q)$ with $0\,Å^{-1} \leq Q \leq 11.75\,Å^{-1}$, blue broken line: corrected $G(r)$ calculated from $S(Q)$ with $0.5\,Å^{-1} \leq Q \leq 11.75\,Å^{-1}$.

Table 3. Comparison of the number density ρ_0 of liquid Ar and SiO_2 glass with/without the Q_{min} termination error correction.

Dataset	Density, ρ_0 (atoms/Å^3)	ρ_0/ρ_{bulk}	Error (%)
Liquid Ar			
Literature value	0.02125	1.0	—
$0.0 < Q \leq 11.75$ Å	0.02086	0.982	1.8
With Q_{min} correction ($0.5 < Q \leq 11.75$ Å)	0.02097	0.987	1.3
Without Q_{min} correction ($0.5 < Q \leq 11.75$ Å)	0.01904	0.896	11.0
SiO_2 glass			
Literature	0.06621	1.0	—
With Q_{min} correction	0.06574	0.993	0.7
Without Q_{min} correction	0.06405	0.967	3.3

correction. The number density of sample ρ_0 is the scale factor that is the residual sum of squares between $G_{obs}(r)$ and ideal $G(r<r_{min}) = -4\pi r\rho_0$ less than $r<r_{min}$.

$$\mathrm{RSS} = \sum_i \left(\alpha(Q_i) - \rho_0 \beta(Q_i)\right)^2. \tag{22}$$

where $\alpha(Q)$ and $\beta(Q)$ are expressed below:

$$\alpha(Q) = \int_0^{r_{min}} G_{obs}(r) \frac{\sin Qr}{Q} dr,$$
$$\beta(Q) = -4\pi \int_0^{r_{min}} r \frac{\sin Qr}{Q} dr. \tag{23}$$

We define the modified $\alpha(Q)$ relatinoship to $\gamma(r)$ that corrects the Q_{min} termination error as follows:

$$\alpha(Q) = \int_0^{r_{min}} \left(G_{obs}(r) + \gamma(r)\right) \frac{\sin Qr}{Q} dr. \tag{24}$$

The comparison of estimated density values with/without the Q_{min} termination error correction are listed in Table 3. Both results for liquid Ar and SiO_2 glass are within 1.5% of the bulk density. The results indicate that the modified density estimation method introducing the Q_{min} termination error correction can improve the accuracy of the estimated number density of a sample compared to that of our previous results[2].

Summary

In this paper, we discuss the standard deviation and termination errors in $G_{obs}(r)$. It has been widely accepted that total scattering profile with a higher measurable Q value provides "*good*" $G_{obs}(r)$. Herein, "*good*" means $G_{obs}(r)$ with high spatial resolution (i.e., narrow peak width). Our result indicates that the Q_{min} value also affects the quality of $G_{obs}(r)$. Since SmartLab can measure total scattering profile over a wide Q-range, we obtain $G(r)$ with narrower peak widths and a minimal Q_{min} termination error, requiring only a simple correction. In the future, we will provide solutions displaying the standard deviation in $G_{obs}(r)$ and the Q_{min} termination error correction in the TXS plugin.

Acknowledgement

The authors would like to thank members of Structure Visualization Group, and Dr. Akihiro Himeda and Dr. Norihiro Muroyama of XRD Application & Software Development for useful discussions.

The authors would like to acknowledge Dr. Beverly Vincent for his careful reading of the manuscript and suggestions.

References

(1) T. Egami and S. J. L. Billinge: Underneath the Bragg Peaks: Structural Analysis of Complex Materials, Second edition, Elsevier, Amsterdam, 2012.
(2) M. Yoshimoto and K. Omote: *J. Phys. Soc. Jpn.*, **91** (2022) 104602. https://doi.org/10.7566/JPSJ.91.104602.
(3) M. Yoshimoto and K. Omote: *Appl. Phys. Exp.,* **16** (2023) 015005. https://doi.org/10.35848/1882-0786/acb2b0.
(4) *Rigaku Journal,* **39** (2023) No. 1, 15–23.
(5) E. Prince Ed.: International Tables for Crystallography Vol. C: Mathematical, Physical and Chemical Tables, 3rd Edition, Wiley, (2004), 599–608.
(6) J. Krogh-Moe: *Acta Cryst.,* **9** (1956), 951–953. https://doi.org/10.1107/S0365110X56002655.
(7) N. Norman: *Acta Cryst.*, **10** (1957), 370–373. https://doi.org/10.1107/S0365110X57001085.
(8) B. J. Thijsse: *J. Appl. Crystallogr.*, **17** (1984), 61–76. https://doi.org/10.1107/S002188988401102X.
(9) B. H. Toby and T. Egami: *Acta Crystallogr.,* **A48** (1992), 336–346. https://doi.org/10.1107/S0108767391011327
(10) B. H. Toby and S. J. L. Billinge: *Acta Crystallogr.*, **A60** (2004), 315–317. https://doi.org/10.1107/S0108767304011754.
(11) E. Lorch: *J. Phys. C*: *Solid State Phys.*, **2** (1969), 229–237. https://doi.org/10.1088/0022-3719/2/2/305.
(12) A. B. Bhatia and D. E. Thornton: *Phys. Rev.*, **B2** (1970), 3004–3012. https://doi.org/10.1103/PhysRevB.2.3004.
(13) J. L. Yarnell, M. J. Katz, R. G. Wenzel and S. H. Koenig: *Phys. Rev.*, **A7** (1973), 2130–2144. https://doi.org/10.1103/PhysRevA.7.2130.